

Response surface optimization of heterogeneous Fenton-like degradation of sulfasalazine using Fe-impregnated clinoptilolite nanorods prepared by Ar-plasma

Alireza Khataee^{1,2} · Soghra Bozorg¹ · Behrouz Vahid³

Received: 12 July 2016 / Accepted: 10 December 2016 / Published online: 11 January 2017
© Springer Science+Business Media Dordrecht 2017

Abstract Optimization of sulfasalazine degradation using the heterogeneous Fenton-like process in batch mode was investigated by response surface methodology. The plasma-treated clinoptilolite (PTC) nanorods were produced from natural clinoptilolite (NC) by Ar glow-discharge plasma owing to its cleaning and sputtering effect generating extra surface area. The PTC and NC catalysts were characterized by XRD, BET, and SEM. The morphology of NC was altered from microparticles to nanorods after plasma modification and consequently the specific surface area increased from 23.92 to 45.16 m²/g. The PTC and NC were modified by Fe-impregnation method. The catalytic performance of Fe-impregnated PTC was significantly higher than Fe-impregnated NC for degradation of sulfasalazine by the process. Central composite design (CCD) approach was performed to develop a non-linear model for determination of the degradation efficiency (DE%). The predicted data for the DE% as a function of operational parameters including initial sulfasalazine concentration (10–50 mg/L), catalyst dosage (0.5–2.5 mg/L), hydrogen peroxide concentration (1–5 mmol/L), and process time (20–60 min) were consistent with the experimental data ($R^2 = 0.945$) after 40 min of the process. The CCD model was also used to estimate the optimized experimental conditions for the sulfasalazine degradation. Environmentally friendly plasma treatment of the NC, low released iron concentration and proper reusability at the mild pH were the essential benefits of the modified PTC.

✉ Alireza Khataee
a_khataee@tabrizu.ac.ir

¹ Research Laboratory of Advanced Water and Wastewater Treatment Processes, Department of Applied Chemistry, Faculty of Chemistry, University of Tabriz, Tabriz 51666-14766, Iran

² Department of Materials Science and Nanotechnology, Near East University, Mersin 10, 99138 Nicosia, North Cyprus, Turkey

³ Department of Chemical Engineering, Tabriz Branch, Islamic Azad University, Tabriz 51579-44533, Iran

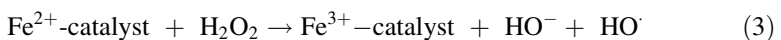
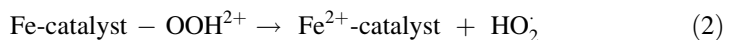
Keywords Nanorods · Natural clinoptilolite · Ar plasma · Sulfasalazine · Heterogeneous Fenton-like

Introduction

In most of pharmaceutical, paper, textile, cosmetic, and food leather industries, large extent of chemicals are manufactured and used at various parts. Discharge of these organic pollutants like drugs to the wastewaters results in persistent contamination of water environments. Also, diverse problems due to their toxicity and carcinogenicity can be immersed in the aquatic life [1]. Sulfasalazine (SSZ), classified as a sulfa drug, is widely applied for treatment of ulcerative colitis, arthritis, and Crohn's disease owing to its antibacterial properties. SSZ has a sulfonamide group and an azo band, which has selected as a model persistent pharmaceutical in the aqueous environment [2].

Development of novel methods for treatment of wastewater is crucial from an environmental point of view. The high efficiency and convenience of advanced oxidation processes (AOPs) make them an appropriate option for oxidizing toxic and resistant chemicals from wastewaters [3–5]. Among diverse AOPs, application of the homogenous Fenton process has been vastly applied in the degradation of various contaminants [3, 5–7]. However, this process has some disadvantages such as narrow acidic pH medium to prevent iron precipitation, sludge formation and catalyst deactivation via generated intermediates [4, 8]. Moreover, homogeneous catalyst separation from the solution and its recycled material restrict Fenton process usage. Use of the heterogeneous Fenton process with no requirement for dissolved catalyst separation and confined leached iron is a practicable way to overcome the above-mentioned problems [9, 10]. However, it should be noted that the heterogeneous Fenton process has main constraints of low active reaction sites and mass transfer. Thus, its catalytic performance can be enhanced by applying nanosized particles instead of micrometer particles since they provide a short diffusion path for organic pollutants [11]. In addition, nanosized particles have larger external surface area and hence further sites for pollutant degradation [12, 13].

Superficial solid Fe ions in the heterogeneous Fenton-type catalysts such as natural and synthetic zeolites [14], laponite [15], pyrite [16], magnetite [17], goethite [18], and pillared clays [19] catalyze the production of HO[•] radicals. The following reactions are involved in the heterogeneous Fenton-like process [20]:



Furthermore, iron-substituted zeolites are effectively applied in the heterogeneous Fenton-like process owing to their physicochemical properties such as stability, crystallinity, and ion-exchange ability [21–23]. Zeolites are crystalline,

porous, and hydrated aluminosilicates [24, 25]; their structure consists of a three-dimensional network of AlO_4^{5-} and SiO_4^{4-} units connected by oxygen atoms [26]. Its structure comprises regular cages with the size of 3–20 Å situated by water molecules and positively charged ions [27–29]. Clinoptilolite, as the natural zeolite, has been extensively applied in research due to its abundance, non-toxicity, and low-cost [22, 30–32]. However, the clinoptilolite has inadequate surface area restricting the mass transfer in the processes [33, 34]. Thus, to enhance its performance, the crystal thickness should be decreased to nanometer scale using different synthetic routes, which generally need toxic precursors and sophisticated equipment [35–37].

Recently, environmentally friendly non-thermal plasma glow discharge, radio frequency, and silent discharge plasmas are applied for surface modifications of various catalysts and formation of different nanostructures to enhance their performance [38–41]. For instance, the stability and activity of the Pd/HZSM-5 catalyst have been amended by the plasma [42]. The selectivity of acetylene hydrogenation enhances by the plasma treated Pd/TiO₂ catalyst [43]. Catalytic ozonation and heterogeneous sono-Fenton processes are employed for treatment of organic dyes using plasma treated magnetite and pyrite, respectively [44, 45].

The heterogeneous Fenton-like process must be optimized to achieve the best implementation. The (CCD) is one of the response surface methods (RSM), which optimizes the response surface using rational number of experiments. The CCD method develops a nonlinear mathematical equation with the appropriate fit for experimental data; it also determines the optimized values for operational parameters leading to an optimum response amount [46]. The CCD method was properly used for modeling and optimization of various water treatment methods such as peroxi-coagulation [47], photocatalysis [48], Fenton [49], photo-Fenton [50], photoelectro-Fenton [51], photoelectro-Fenton/citrate/TiO₂ [52], and heterogeneous Fenton processes [53].

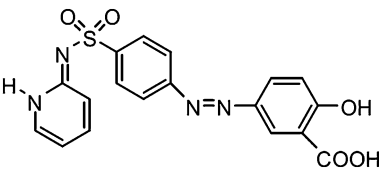
The aim of this study was production of nanosized clinoptilolite from NC by Ar glow discharge plasma. The PTC and NC were specified by X-ray diffraction (XRD), Brunauer–Emmett–Teller (BET), and scanning electron microscopy (SEM) methods. Then, the PTC and NC were modified by Fe-impregnation method, and Fe amount in the bulk of the catalysts was measured by inductively coupled plasma (ICP) technique. The obtained samples were compared for the SSZ degradation by the heterogeneous Fenton-like degradation. Finally, the degradation of SSZ was optimized by the CCD method using the modified PTC. The experimental parameters in the CCD were chosen as initial sulfasalazine concentration, catalyst dosage, hydrogen peroxide concentration, and reaction time.

Experimental

Chemicals

All chemicals were of analytical grade and applied without purification. H₂O₂ (30%), FeCl₃·6H₂O, H₂SO₄, and NaOH were provided from Merck Co. (Germany).

Table 1 Characteristics of the sulfasalazine

Chemical structure	Molecular formula	λ_{max} (nm)	M_w (g/mol)
	$C_{18}H_{14}N_4O_5S$	398.39	360

The clinoptilolite were supplied from Mianeh region (Kan Azar Co., Iran). The SSZ was obtained from Mehrdarou pharmaceutical Co. (Tehran, Iran); its properties are presented in Table 1.

Plasma treated clinoptilolite preparation

The plasma treatment set-up for is demonstrated in Fig. 1.

Distilled water was used for washing of the clinoptilolite and then the particles were dried at 60 °C for 24 h. The sample (1 g) was placed in a Pyrex tube with size of 40 × 5 cm as the plasma reactor. The non-thermal glow discharge plasma is formed by two aluminum electrodes linked to a direct current (DC) with voltage of 1200 V. The Ar gas was fed to the reactor with a flow of 4 cm³/s and 26 Pa for 45 min.

Characterization instruments

The clinoptilolite phase before and after plasma was identified by the XRD analysis (PANalytical X'Pert PRO diffractometer). The pore volume and surface area of the NC and PTC were determined using nitrogen adsorption/desorption at 77 K by a Micromeritics ASAP-2010 instrument. The morphology and size of the NC and PTC samples were obtained using the SEM (S-4200, Hitachi, Japan). The size distribution of the PTC was determined by microstructure distance measurement software (Nahamin Pardazan Asia Co., Iran) using the SEM micrograph.

Preparation of Fe-impregnated clinoptilolite

The Fe-impregnated clinoptilolite nanorods were produced by mixing of the PTC (50 g) with $FeCl_3 \cdot 6H_2O$ solution (0.125 M, 150 mL) and NaOH solution (2 M, 200 mL), separately. The NaOH solution was added to the solution under stirring to adjust the pH at 10.

The sample was put in a water bath (60 °C) for 6 h. Then, it was washed with the distilled water and dried by an oven (60 °C) for 24 h. The mentioned method was

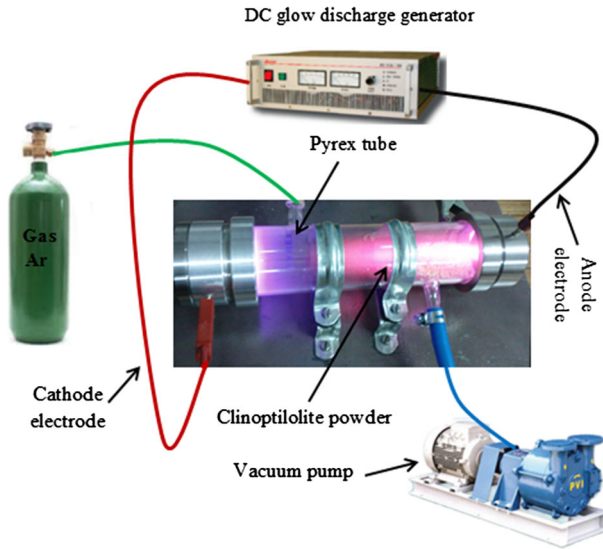


Fig. 1 Ar glow-discharge plasma set-up

applied for three times to yield the Fe-impregnated PTC. The same procedure was carried out for the NC to obtain the Fe-impregnated NC.

Heterogeneous Fenton-like procedure

All runs were performed in a batch mode under magnetic stirring. In each run, the SSZ solution (500 mL) with pH 5 and concentration containing known H_2O_2 concentration and catalyst dosage was treated. The pH was adjusted by H_2SO_4 and NaOH solutions. To measure the remaining concentration of the drug at a definite process time, 3 mL of the sample was withdrawn and degradation efficiency was calculated by $(A_0 - A_t)/A_0$ where A_0 and A_t were the initial absorbance and absorbance after the treatment of the drug at $\lambda_{\text{max}} = 360$ nm, respectively. The drug absorbance was measured by an UV-Vis spectrophotometer (Lightwave S2000, England).

CCD design of experiments

The CCD is mixture of mathematical and statistical techniques to optimize a process. This approach results in the less experimental work, chemicals, and time [54]. In this research, the influence of four principal operational factors including initial sulfasalazine concentration (mg/L) (X_1), catalyst dosage (mg/L) (X_2), hydrogen peroxide concentration (mmol/L) (X_3), and reaction time (min) (X_4) on the SSZ degradation using the heterogeneous Fenton-like process by the modified PTC was studied. Totally 31 runs have been carried out consisting of 16 cubic points, eight axial points, and seven repetitions at the central point. Minitab 15.1.1 was applied to evaluate the obtained data. The X_i values are coded as x_i by Eq. 4:

Table 2 Coded and actual values of variables of the experimental design

Variables	Ranges and levels				
	-2	-1	0	+1	+2
Sulfasalazine concentration (mg/L) (X_1)	50	40	30	20	10
Catalyst concentration (g/L) (X_2)	2.5	2.0	1.5	1.0	0.5
H ₂ O ₂ concentration (mmol/L) (X_3)	5	4	3	2	1
Reaction time (min) (X_4)	60	50	40	30	20

$$x_i = \left(\frac{X_i - X_0}{\delta X} \right) \quad (4)$$

where X_0 is the X_i value at the center point and δX represents the change of step [55, 56]. The experimental levels and ranges for the operational parameters are given in Table 2, which were selected based on a few preliminary experiments.

Results and discussion

Characterization and production of the PTC

Figure 2a, b shows XRD spectra of the NC and PTC. In these patterns, the XRD peaks at 2θ values of 10.9° , 17.53° , 22.7° , and 27.63° are consistent with the clinoptilolite results (JCPDS card 83-1260) [30, 57]. Moreover, feldspar, biotite, and quartz phases are recognized in minor amounts in the XRD spectra [23]. Based on the manufacturer's specifications, the clinoptilolite quantity is more than 90% (w/w). Comparison between standard clinoptilolite spectrum and these two patterns confirmed the stableness of its crystal structure after the Ar plasma treatment. Moreover, as can be observed in Fig. 2b, some peaks are slightly shifted to the lower 2θ and broaden; their intensities also decrease. These observations are owing to less ordered zeolite framework and smaller plasma treated particles and consistent with the previous studies in the field of plasma treatment [30, 42, 58, 59].

The BET isotherm model was applied to describe the obtained results from the N₂ adsorption/desorption isotherm of the NC and PTC. The pore volume and specific surface area of the NC were calculated as $1.43 \text{ cm}^3/\text{g}$ and $23.92 \text{ m}^2/\text{g}$, which enhanced to $2.21 \text{ cm}^3/\text{g}$ and $45.16 \text{ m}^2/\text{g}$, respectively. This enhancement confirmed the thickness reduction of the crystal and development of the clinoptilolite nanorods.

The SEM images of the NC and PTC are displayed in Fig. 3. They indicate the development of nanorods in the PTC (Fig. 3b) from the bulky structure of NC (Fig. 3a) after the plasma treatment. As observed in Fig. 4, the average diameter of these nanorods is 30–50 nm. These nanorods enhance the surface area and thus the performance of PTC, which also was verified by the XRD and BET analyses results.

Plasma, noted as the fourth state of matter, includes electrons, ions, photons, excited species, and neutral species, which can cause engraving and sputtering

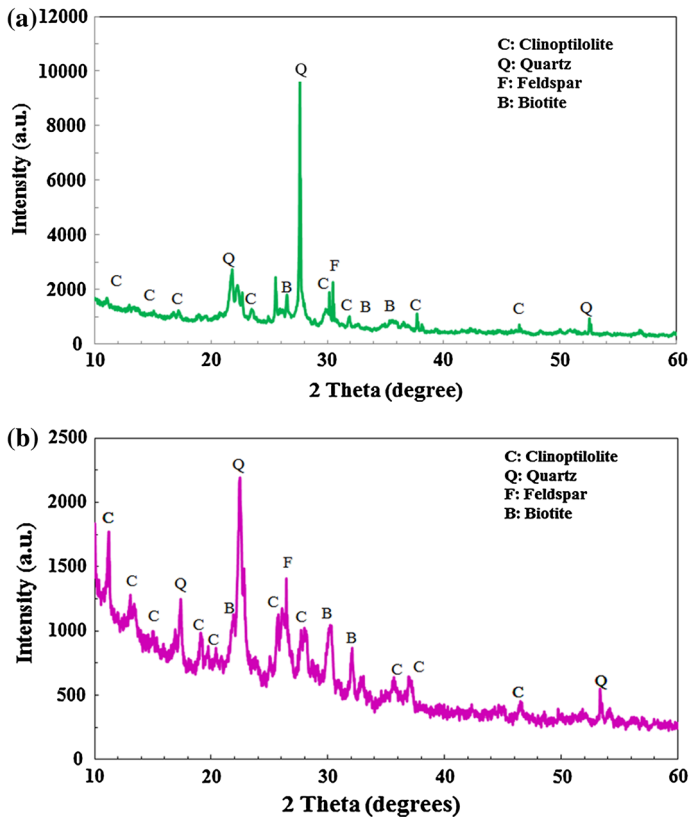


Fig. 2 XRD patterns of the **a** NC and **b** PTC

effects [60, 61]. It is proven that the thermal effect during plasma treatments does not alter the catalyst structure and performance [58, 61]; therefore, the nonthermal plasma treatment performance has been explained by an electronic mechanism. First, the electrons are trapped by the catalyst particles by acting as sinks of the electron; it is confirmed by the considerable decline of electron density in the presence of catalyst powders. Next, the trapped electrons generate a sheath of plasma about the catalyst, which is repulsed effectively by the electrons of plasma zone. Simultaneously, the trapped electrons on the catalyst repulse each other powerfully. Consequently, owing to the repulsive forces in the catalyst particle and plasma sheath around it, some elements bonds are stretched out, split, and distorted leading to the structural changes [58, 61].

Comparison of heterogeneous catalysts activity in the Fenton-like process

Adsorption of SSZ by the Fe-impregnated NC and PTC catalysts are lower than 10% in the dark. Furthermore, hydrogen peroxide has an insignificant influence on drug degradation (4%) after 60 min. Figure 5 shows the performance of Fe-

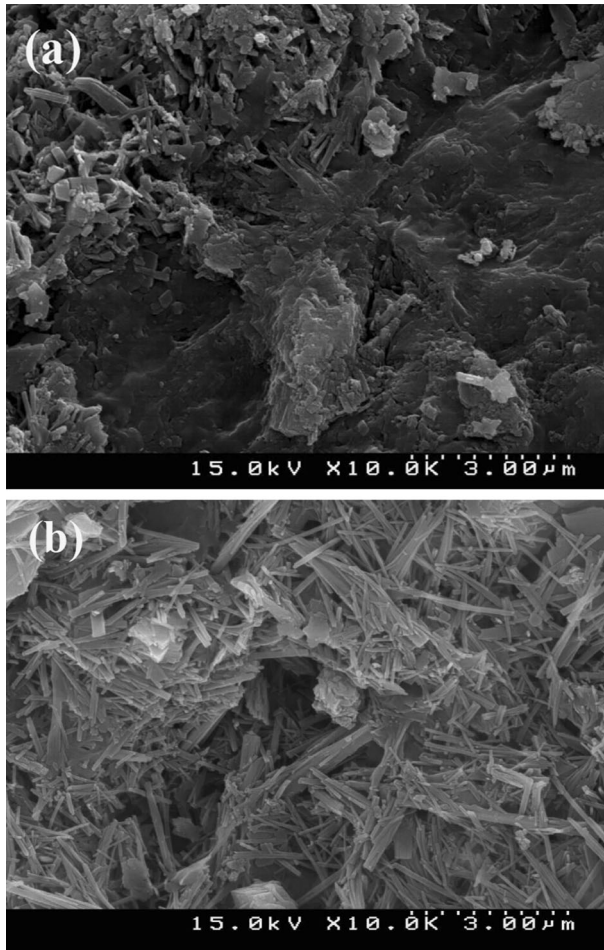


Fig. 3 SEM images of the **a** NC and **b** PTC

impregnated catalysts in the degradation of the model drug contaminant at identical operational parameters. The DE% of SSZ was 33.93 and 96.67% for the Fe-impregnated NC and PTC after 40 min of the treatment process, respectively. This confirmed the proper potential of the modified PTC in the Fenton-like process. This was owing to the enhanced specific surface area and hence more iron impregnation capacity of the PTC compared to NC, which was verified by ICP analysis. According to the ICP data, the iron amount in the Fe-impregnated samples was 7.5 and 15.3 mg/g for NC and PTC, respectively. Moreover, Fig. 6 shows the reusability the Fe-impregnated catalysts in degradation of SSZ, after five repeated runs, which is a significant factor from a practical point of view. As observed in Fig. 6, the both catalysts exhibit appropriate stability during the five cycles of the process.

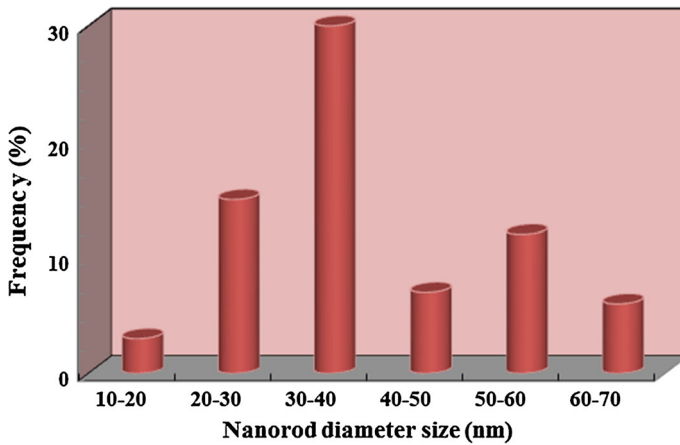


Fig. 4 Size distribution plots of the PTC

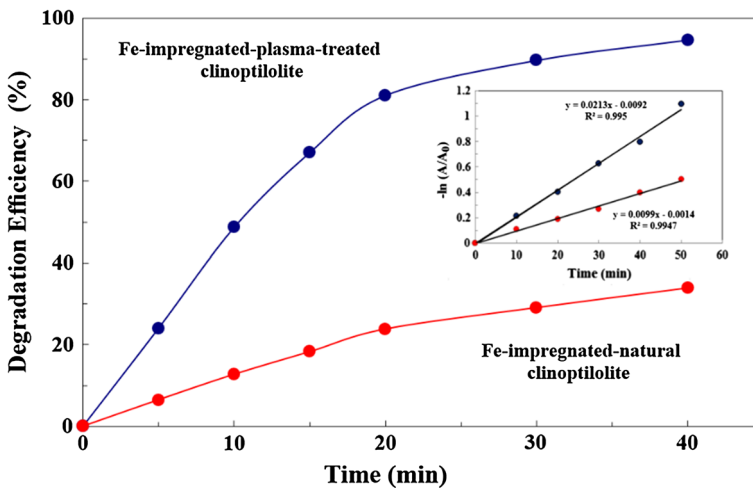


Fig. 5 Evaluating the catalytic properties of Fe-impregnated-natural and Fe-impregnated-plasma-treated clinoptilolite in heterogeneous Fenton-like process for removal of 20 mg/L SSZ solution in the presence of 3 mmol/L H_2O_2 , 2.0 g/L catalyst and pH = 5. The inset plot was depicted according to the pseudo-first order kinetic assumption for the SSZ degradation

The heterogeneous Fenton-like process obey pseudo-first order kinetic alike to the other researches [2, 45, 62]. The apparent pseudo-first order rate constants (k_{app}) for the SSZ degradation are calculated from $-\ln(A/A_0)$ versus time (t) plots as 0.0099 and 0.0213 min^{-1} , for Fe-impregnated NC and PTC, respectively. The solid lines with appropriate correlation coefficients (R^2) confirm the suggested kinetic (inset plot figure of Fig. 5).

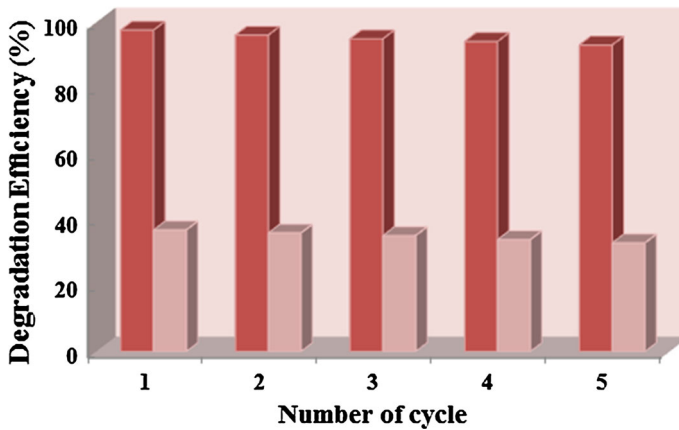


Fig. 6 Reusability behavior of **a** NC and **b** plasma-treated clinoptilolite in heterogeneous Fenton-like process for removal of 20 mg/L SSZ solution in the presence of 3 mmol/L H_2O_2 , 2.0 g/L catalyst and pH = 5

Optimization of the heterogeneous Fenton-like degradation of sulfasalazine

In this section, Minitab 16 was used to plan a CCD matrix and nonlinear regression analysis of the obtained data for the heterogeneous Fenton-like process using the modified PTC [63]; a polynomial model was developed to estimate the response (DE%) as a function of the operational variables via a second order equation:

$$DE\% = b_0 + b_1x_1 + b_2x_2 + b_3x_3 + b_4x_4 + b_{12}x_1x_2 + b_{13}x_1x_3 + b_{14}x_1x_4 + b_{23}x_2x_3 + b_{24}x_2x_4 + b_{34}x_3x_4 + b_{11}x_1^2 + b_{22}x_2^2 + b_{33}x_3^2 + b_{44}x_4^2 \quad (5)$$

By substituting of the coefficients values in the above equation, the CCD equation was obtained as the follows:

$$DE\% = 88.97 - 5.40x_1 - 14.00x_2 + 44.89x_3 - 1.18x_4 + 1.12x_1x_2 - 3.87x_1x_3 + 0.032x_1x_4 - 6.69x_2x_3 - 0.11x_2x_4 - 0.20x_3x_4 + 0.04x_1^2 + 7.24x_2^2 - 3.41x_3^2 + 0.03x_4^2 \quad (6)$$

Analysis of variance (ANOVA) is the another method to examine the CCD model significance and adequacy (Table 3) [64]. The ANOVA separates the results variations to two classes related to the model and residual errors, respectively. F value is described as the ratio of the mean squares of the model and residual errors indicating if the model variation is important or not in comparison with the residual error. The model adequacy is verified when the F value is higher than the tabulated one for a definite number of degrees of freedom in the model at a significance level of α . The F value was calculated as 19.76 by the software in this study, which was

Table 3 Analysis of variance (ANOVA) for fit of degradation efficiency from central composite design

Source of variations	Sum of squares	Degrees of freedom	Adjusted mean square	<i>F</i> value	<i>p</i> value
Regression	9553.2	14	682.37	19.76	0.000
Residuals	552.6	16	34.54	–	0.000
Lack of fit	415.5	10	41.55	1.82	0.24
Pure error	137.1	6	22.85	–	–
Total	10,105.8	30	–	–	–

$$R^2 = 0.945$$

passably higher than tabulated *F* value at 95% (2.352) significance verifying the CCD model accuracy [65]. The *F* values of the independent variables including initial drug concentration, H₂O₂ concentration, process time and catalyst dosage are calculated as 24.68, 17.04, 8.98, and 0.41, respectively. This order revealed the importance of the independent variables on the process. The suitable prediction of model was confirmed by the data of Table 4.

After the model development, it can be applied not only for prediction of DE%, but also for determination of desired conditions for the drug degradation. The optimized conditions for entire drug degradation are specified as hydrogen peroxide concentration of 3 mmol/L, initial SSZ concentration of 20 mg/L, pH 5, and catalyst dosage 2 g/L after 40 min of the process; DE% is obtained experimentally as 98.67%, which is the acceptable prediction.

The CCD plots and effect of operational parameters

It is well-established that the pH is one of the most important parameters governing pollutants treatment in the both homogeneous and heterogeneous Fenton processes [15, 66]. Moreover, the HO· oxidation potential increases in the smaller pH ranges [67], which has been determined as 1.64 and 2.59 V versus normal hydrogen electrode (NHE) at pH 14 and 0, respectively [68]. The effect of initial solution pH (3–9) on the degradation of SSZ was studied (Fig. 7). DE% declined by increasing of the pH, which can be related to the requirement of acidic medium for Fenton reaction implementation (Eq. 1). The particular environment of Fe³⁺ with strong electrostatic forces exists inside the structural pores of the modified PTC. The

Table 4 Optimum operating conditions of the process variables

Variable	Optimum values
Initial SSZ concentration (mg/L) (<i>X</i> ₁)	20
Catalyst concentration (g/L) (<i>X</i> ₂)	2
H ₂ O ₂ concentration (mmol/L) (<i>X</i> ₃)	3
Reaction time (min) (<i>X</i> ₄)	40
Experimental DE (%)	93.00
Predicted DE (%)	89.01

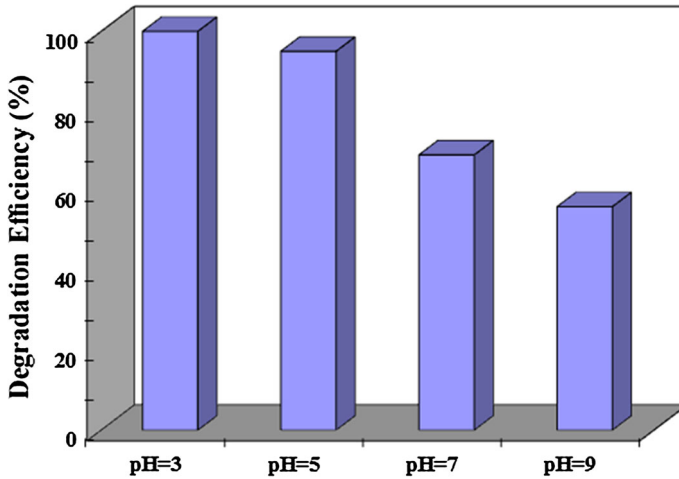


Fig. 7 Effect of the initial pH of solution on SSZ degradation efficiency by the heterogeneous Fenton-like process; [SSZ] = 20 mg/L, [Catalyst] = 2.0 g/L, and [H₂O₂] = 3 mmol/L

interaction of Fe³⁺ ions with negative framework groups of Si–O[−]–Al, Si–O[−] and Al–O[−] can slow down the iron hydroxides precipitation even in basic mediums [57]. These interactions caused the heterogeneous Fenton-like process to be performed at milder acidic medium, which is one of the primary benefits of this process. Consequently, pH 5 was selected for the CCD optimization experiments owing to the insignificant DE% compared to pH 3. Moreover, the iron leached into the solution was low at various pHs as shown in Fig. 8, which revealed that the main iron amount remained in the catalyst structure based on the literature [4, 69].

The dependence of DE% on SSZ amount was investigated by increasing of the drug initial concentration from 10 to 50 mg/L, with hold values of 2 g/L PTC and 3 mmol/L

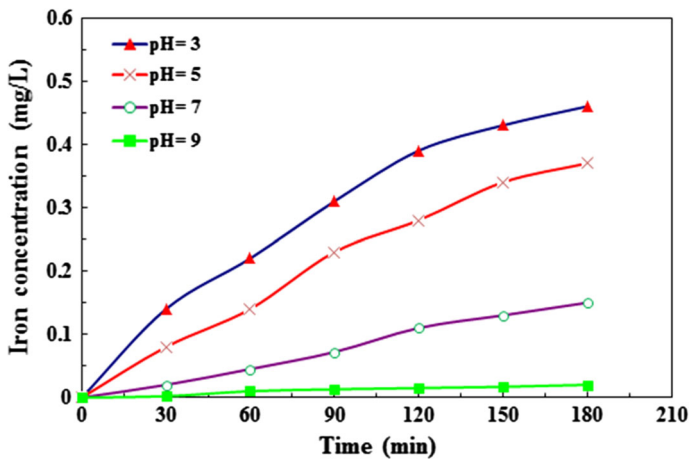


Fig. 8 The leached iron concentration at various pH; [Catalyst] = 2.0 g/L

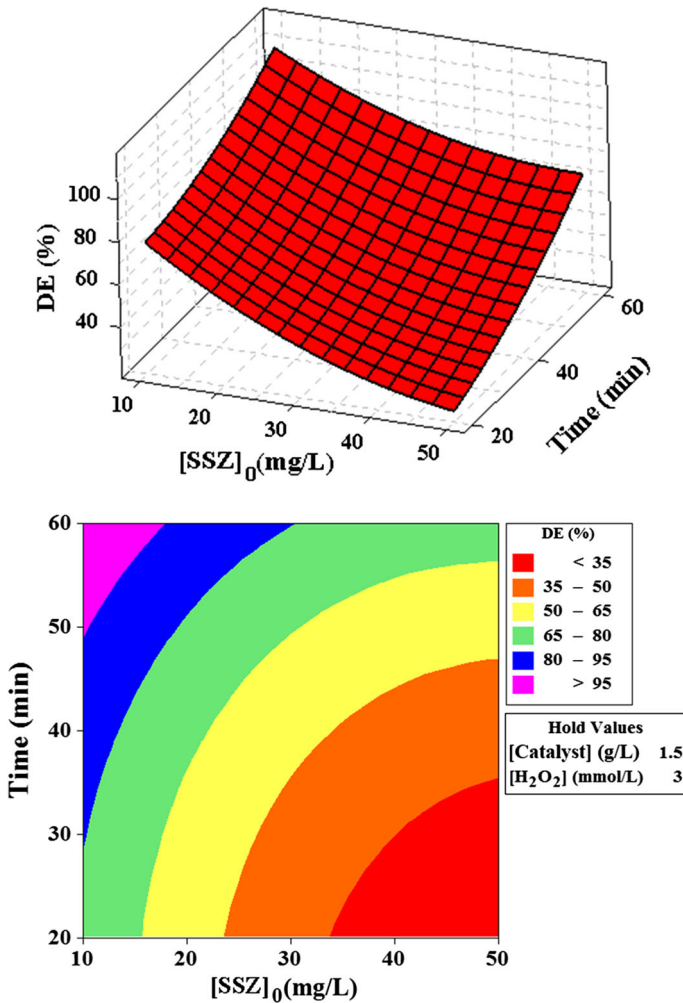


Fig. 9 The response surface plots of DE% as a function of initial drug concentration (mg/L) and process time (min)

H_2O_2 (Fig. 9). A distinct content of HO^\cdot radicals were generated under certain experimental conditions of the process. However, when the SSZ concentration and its degradation intermediates increased, the constant amount of generated HO^\cdot radicals was not sufficient to treat higher concentrations of them. As a consequence, DE% of SSZ decreased by increasing of the drug concentration [3, 70].

The effect of PTC amount on the SSZ degradation was studied by varying the catalyst dosage from 0.5 to 2.5 g/L with hold values of 20 mg/L SSZ and 3 mmol/L H_2O_2 (Fig. 10). It can be observed that with the catalyst dosage increasing, the DE% increased, which could be related to the higher adsorption of SSZ and H_2O_2 owing to the enhanced active sites. Hence, the production of HO^\cdot radicals as the oxidizing agent of the drug increased under the applied experimental conditions [5, 14].

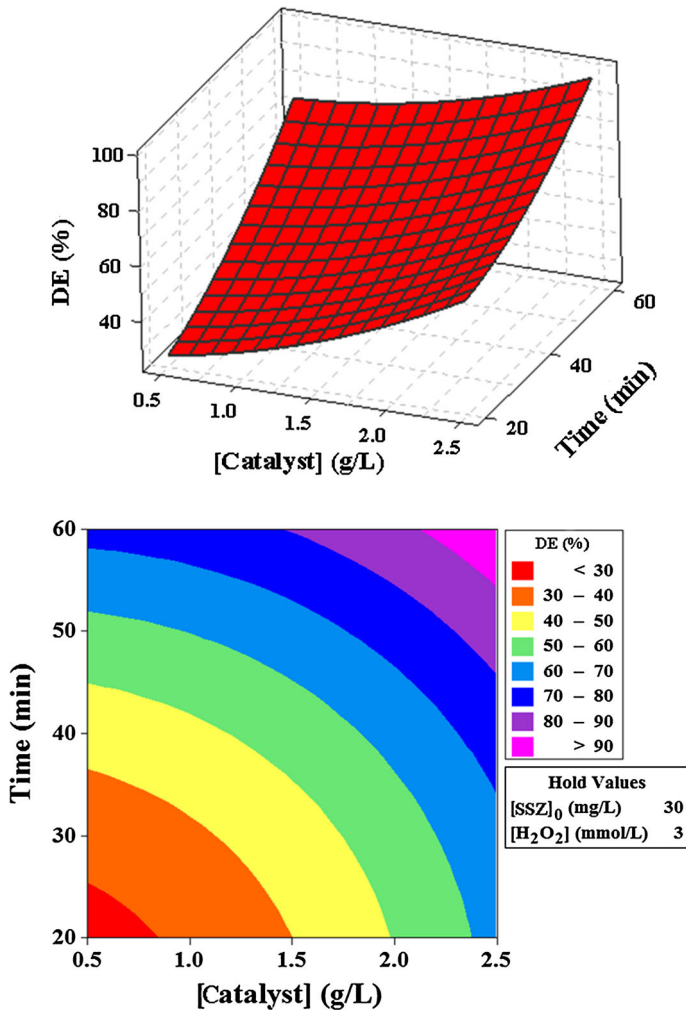


Fig. 10 The response surface plots of the DE% as the function of catalyst dosage (g/L) and process time (min)

The H_2O_2 concentration optimization is significant from economic viewpoint due to the cost of oxidant. When H_2O_2 concentration changed from 1 to 5 mmol/L, the DE% increased until an optimized value and afterward declined with the hold values of 2 g/L PTC and 20 mg/L SSZ (Fig. 11). This was due to the generation of more HO^\cdot radicals from the H_2O_2 dissociation by the PTC catalyst. But further H_2O_2 amount decreased DE% due to H_2O_2 scavenging influence on the active radicals [Eqs. (7) and (8)] [71]. It should be noted that the produced hydroperoxyl radical (HO_2^\cdot) in the presence of excess H_2O_2 was less reactive than HO^\cdot radicals [72]. A similar trend has been also observed for the direct blue 71 and acid red 66 degradations in the aqueous solution via the Fenton process [73].

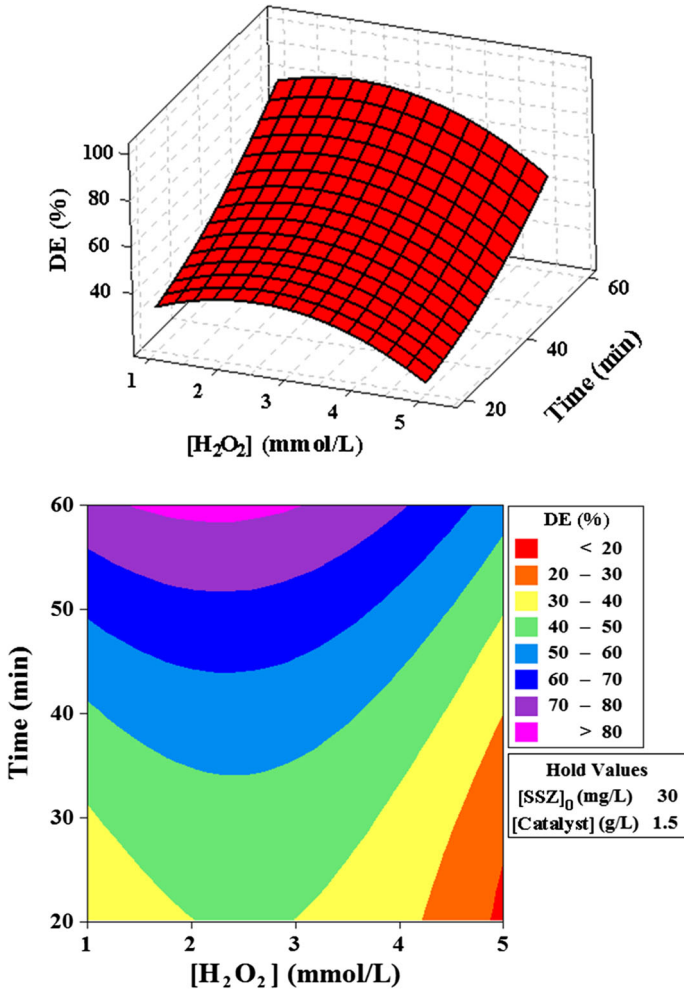
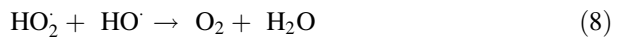
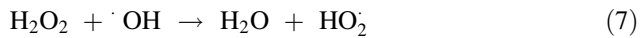


Fig. 11 The response surface plots of the DE% as the function of H₂O₂ concentration (mmol/L) and process time (min)



Conclusions

NC was modified to the clinoptilolite nanorods by the environmentally friendly Ar glow discharge plasma treatment. The XRD, BET, and SEM results verified the crystallinity, nanorod structure, and enhanced specific surface area of the plasma-treated catalyst. The formation of the modified catalyst was explained by the

electronic mechanism of plasma. Fe-impregnation method was used to modify the PTC and NC. The catalytic performance of the modified NC and PTC demonstrated that the drug degradation efficiency was considerably enhanced from 33.93%, in the presence of NC, to 96.67% by using the PTC after 40 min. Finally, the nonlinear model of was obtained as a function of initial drug concentration, catalyst dosage, hydrogen peroxide concentration, and reaction time, for prediction of the degradation efficiency and optimization of the heterogeneous Fenton-like process. The results demonstrated that the estimated amounts were in good agreement with the experimental data with $R^2 = 0.945$, and the optimized conditions for the drug treatment were predicted as $[SSZ] = 20 \text{ mg/L}$, $[PTC] = 2 \text{ g/L}$, $[\text{H}_2\text{O}_2] = 3 \text{ mmol/L}$, and reaction time = 40 min. The modified catalysts showed proper reusability with low leached iron at the milder operating pH 5.

Acknowledgements The authors thank the University of Tabriz for all support.

References

1. A.R. Khataee, M. Fathinia, S. Aber, M. Zarei, J. Hazard. Mater. **181**, 1–3 (2010)
2. A. Khataee, S. Arefi-Oskoui, M. Fathinia, A. Fazli, A. Shahedi Hojaghan, Y. Hanifehpour, S.W. Joo, J. Ind. Eng. Chem. **30**, 134–146 (2015)
3. M. Neamtu, C. Zaharia, C. Catrinescu, A. Yediler, M. Macoveanu, A. Kettrup, Appl. Catal. B Environ. **48**, 4 (2004)
4. M. Dukkanci, G. Gunduz, S. Yilmaz, R.V. Prihoduko, J. Hazard. Mater. **181**, 1–3 (2010)
5. N.N. Fathima, R. Aravindhan, J.R. Rao, B.U. Nair, Chemosphere **70**, 6 (2008)
6. A.R. Khataee, M. Safarpour, A. Naseri, M. Zarei, J. Electroanal. Chem. **672**, 1–62 (2012)
7. S. Rahim Pouran, A.R. Abdul Aziz, W. Mohd Ashri Daud, J. Ind. Eng. Chem. **21**, 53–69 (2015)
8. B. Ahmed, E. Limem, A. Abdel-Wahab, B. Nasr, Ind. Eng. Chem. Res. **50**, 11 (2011)
9. M. Sheydaei, S. Aber, A. Khataee, J. Mol. Catal. A Chem. **392**, 8–15 (2014)
10. A. Khataee, H. Aleboyeh, M. Sheydaei, A. Aleboyeh, Res. Chem. Intermed. **42**, 2 (2016)
11. M. Sheydaei, A. Khataee, Ultrason. Sonochem. **27**, 616–622 (2015)
12. C. Yin, Y. Wei, F. Wang, Y. Chen, Mater. Lett. **98**, 42–46 (2013)
13. Z. Cheng, S. Han, W. Sun, Q. Qin, Mater. Lett. **95**, 193–196 (2013)
14. M. Tekbas, H.C. Yatmaz, N. Bektas, Microporous Mesoporous Mater. **115**, 3 (2008)
15. B. Iurascu, I. Siminiceanu, D. Vione, M.A. Vicente, A. Gil, Water Res. **43**, 5 (2009)
16. W. Wang, Y. Qu, B. Yang, X. Liu, W. Su, Chemosphere **86**, 4 (2012)
17. X. Liang, Y. Zhong, H. He, P. Yuan, J. Zhu, S. Zhu, Z. Jiang, Chem. Eng. J. **191**, 177–184 (2012)
18. Z.-R. Lin, L. Zhao, Y.-H. Dong, Chemosphere **141**, 7–12 (2015)
19. Q. Chen, P. Wu, Z. Dang, N. Zhu, P. Li, J. Wu, X. Wang, Sep. Purif. Technol. **71**, 3 (2010)
20. S. Navalon, M. Alvaro, H. Garcia, Appl. Catal. B Environ. **99**, 1–2 (2010)
21. M.L. Rache, A.R. Garcia, H.R. Zea, A.M.T. Silva, L.M. Madeira, J.H. Ramirez, Appl. Catal. B Environ. **6**, 557–572 (2013)
22. M. Kragovic, A. Dakovic, Z. Sekulic, M. Trgo, M. Ugrina, J. Peric, G.D. Gatta, Appl. Surf. Sci. **258**, 8 (2012)
23. Z. Ozcelik, G.S.P. Soyulu, I. Boz, Chem. Eng. J. **155**, 1–2 (2009)
24. M. Qiu, C. Qian, J. Xu, J. Wu, G. Wang, Desalination **243**, 1–3 (2009)
25. H. Faghiehian, M. Talebi, M. Pirouzi, J. Iran. Chem. Soc. **5**, 394 (2008)
26. E. Chmielewska, E. Samajova, J. Kozac, Turk. J. Chem. **26**, 281 (2002)
27. M. Hernandez, F. Rojas, V. Lara, J. Porous Mater. **7**, 443–454 (2000)
28. T. Sen, S. Jana, S. Koner, A. Patra, J. Phys. Chem. C **114**, 46 (2010)
29. M. Danish, X. Gu, S. Lu, M. Xu, X. Zhang, X. Fu, Y. Xue, Z. Miao, M. Naqvi, M. Nasir, Res. Chem. Intermed. **42**, 6959–6973 (2016)
30. M. Akgul, A. Karabakan, Microporous Mesoporous Mater. **131**, 1–3 (2010)

31. A.S.M. Junaid, M. Rahman, H. Yin, W.C. McCaffrey, S.M. Kuznicki, *Microporous Mesoporous Mater.* **144**, 1–3 (2011)
32. A. Arimi, M. Farhadian, A.R. Solaimany Nazar, M. Homayoonfal, *Res. Chem. Intermed.* **42**, 5 (2016)
33. N.L. Chauhan, J. Das, R.V. Jasra, P.A. Parikh, Z.V.P. Murthy, *Mater. Lett.* **74**, 115–117 (2012)
34. L. Wang, W. Yang, C. Xin, F. Ling, W. Sun, X. Fang, R. Yang, *Mater. Lett.* **69**, 16–19 (2012)
35. Z. Xue, J. Ma, T. Zhang, H. Miao, R. Li, *Mater. Lett.* **68**, 1–3 (2012)
36. O.A. Abdel Moamen, I.M. Ismail, N. Abdelmonem, R.O. Abdel Rahman, *J. Taiwan. Inst. Chem. Eng.* **55**, 133–144 (2015)
37. G. Wu, W. Wu, X. Wang, W. Zan, W. Wang, C. Li, *Microporous Mesoporous Mater.* **180**, 187–195 (2013)
38. C.J. Liu, J. Zou, K. Yu, D. Cheng, Y. Han, J. Zhan, C. Ratanatawanate, B.W.L. Jang, *Pure Appl. Chem.* **78**, 6 (2006)
39. X. Zhang, W.-J. Sun, W. Chu, *Fuel Chem. Technol.* **41**, 1 (2013)
40. J. Van Durme, J. Dewulf, C. Leys, H. Van Langenhove, *Appl. Catal. B Environ.* **78**, 3–4 (2008)
41. S. Tang, N. Lu, J.K. Wang, S.K. Ryu, H.S. Choi, *J. Phys. Chem. C* **111**, 4 (2007)
42. C.-J. Liu, K. Yu, Y.-P. Zhang, X. Zhu, F. He, B. Eliasson, *Appl. Catal. B* **47**, 2 (2004)
43. Y. Li, B.W.L. Jang, *Appl. Catal. A* **392**, 1–2 (2011)
44. M. Taseidifar, A. Khataee, B. Vahid, S. Khorram, S.W. Joo, *J. Mol. Catal. A Chem.* **404–405**, 218–226 (2015)
45. A. Khataee, P. Gholami, B. Vahid, *Ultrason. Sonochem.* **29**, 213–225 (2016)
46. R.D.C. Soltani, A. Rezaee, A.R. Khataee, M. Safari, *J. Ind. Eng. Chem.* **20**, 4 (2014)
47. M. Zarei, A. Niaei, D. Salari, A. Khataee, *J. Hazard. Mater.* **173**, 1–3 (2010)
48. R. Marandi, M. Khosravi, M. Olya, B. Vahid, M. Hatami, *Micro Nano Lett.* **6**, 11 (2011)
49. A. Saldana-Robles, R. Guerra-Sanchez, M.I. Maldonado-Rubio, J.M. Peralta-Hernandez, *J. Ind. Eng. Chem.* **20**, 3 (2014)
50. P. Palaniandy, H.B.A. Aziz, S. Feroz, *J. Environ. Chem. Eng.* **3**, 1117–1124 (2015)
51. A.R. Khataee, M. Zarei, S.K. Asl, *J. Electroanal. Chem.* **648**, 2 (2010)
52. A. Khataee, H. Marandizadeh, B. Vahid, M. Zarei, S.W. Joo, *Chem. Eng. Process. Process Intensif.* **73**, 103–110 (2013)
53. S. Fathinia, M. Fathinia, A.A. Rahmani, A. Khataee, *Appl. Surf. Sci.* **327**, 190–200 (2015)
54. A.R. Khataee, M. Zarei, L. Moradkhannejhad, *Desalination* **258**, 1–3 (2010)
55. A. Khataee, A. Khataee, M. Fathinia, B. Vahid, S.W. Joo, *J. Ind. Eng. Chem.* **19**, 6 (2013)
56. A.R. Esfahani, A.F. Firouzi, G. Sayyad, A. Kiasat, L. Alidokht, A.R. Khataee, *Res. Chem. Intermed.* **40**, 1 (2014)
57. M.K. Doula, *Chemosphere* **67**, 4 (2007)
58. C.J. Liu, J. Zou, K. Yu, D. Cheng, Y. Han, J. Zhan, C. Ratanatawanate, B.W.L. Jang, *Pure Appl. Chem.* **78**, 1227–1238 (2006)
59. C.J. Liu, D.G. Cheng, Y.P. Zhang, K.L. Yu, Q. Xia, J.G. Wang, X.L. Zhu, *Catal. Surv. Asia* **8**, 2 (2004)
60. H.-H. Kim, Y. Teramoto, N. Negishi, A. Ogata, *Catal. Today* **256**, 13–22 (2015)
61. C.J. Liu, G.P. Vissokov, B.W.L. Jang, *Catal. Today* **72**, 3–4 (2002)
62. S. Karthikeyan, V.K. Gupta, R. Boopathy, A. Titus, G. Sekaran, *J. Mol. Liq.* **173**, 153–163 (2012)
63. M.O. Saeed, K. Azizli, M.H. Isa, M.J.K. Bashir, *J. Water. Process. Eng.* **8**, 7–16 (2015)
64. A.V. Schenone, L.O. Conte, M.A. Botta, O.M. Alfano, *J. Environ. Manag.* **155**, 177–183 (2015)
65. M.A. Bezerra, R.E. Santelli, E.P. Oliveira, L.S. Villar, L.A. Escalera, *Talanta* **76**, 5 (2008)
66. M.D.G. Luna, M.L. Veciana, J.I. Colades, C.-C. Su, M.-C. Lu, *J. Taiwan Inst. Chem. E* **45**, 2 (2014)
67. M. Sheydaei, S. Aber, A. Khataee, *J. Ind. Eng. Chem.* **20**, 1772–1778 (2013)
68. A. Babuponnusami, K. Muthukumar, *J. Environ. Chem. Eng.* **2**, 1 (2014)
69. M. Bayat, M. Sohrabi, S.J. Royae, *J. Ind. Eng. Chem.* **18**, 3 (2012)
70. J.R. Idel Aouad, M. Valiente, A. Yaacoubi, B. Tanouti, M. Lopez Mesas, *J. Hazard. Mater.* **186**, 745–750 (2011)
71. L. Xu, J. Wang, *Appl. Catal. B* **123–124**, 117–126 (2012)
72. E. Neyens, J. Baeyens, *J. Hazard. Mater.* **98**, 1–3 (2003)
73. S. Tunç, T. Gürkan, O. Duman, *Chem. Eng. J.* **181–182**, 431–442 (2012)